Adsorption and diffusion of hydrogen and methane in 2D covalent organic frameworks

ARTICLE *in* MICROPOROUS AND MESOPOROUS MATERIALS · DECEMBER 2008

Impact Factor: 3.45 · DOI: 10.1016/j.micromeso.2008.05.023

2 AUTHORS:

Giovanni Garberoglio
Fondazione Bruno Kessler
60 PUBLICATIONS **1,165** CITATIONS
SEE PROFILE

Renzo Vallauri
Università degli Studi di Trento
130 PUBLICATIONS **2,134** CITATIONS
SEE PROFILE

Microporous and Mesoporous Materials 116 (2008) 540–547

Contents lists available at ScienceDirect

Microporous and Mesoporous Materials

journal homepage: www.elsevier.com/locate/micromeso

Adsorption and diffusion of hydrogen and methane in 2D covalent organic frameworks

G. Garberoglio *, R. Vallauri

CNISM and Dipartimento di Fisica dell'Università di Trento, Via Sommarive 14, 38100 Povo, TN, Italy

ARTICLE INFO

Article history:
Received 3 April 2008
Received in revised form 7 May 2008
Accepted 8 May 2008
Available online 25 May 2008

Keywords:
Covalent organic frameworks
Adsorption
Transport
Hydrogen
Methane

ABSTRACT

We report computer simulation results for adsorption and diffusion of hydrogen and methane in recently synthesized 2D covalent organic frameworks. Our model, based on classical force fields, is able to reproduce fairly well the experimental adsorption isotherms of argon at $T = 87$ K.
The calculated adsorption isotherms of H_2 and CH_4 at $T = 77$ K and $T = 298$ K show that the uptake to be expected for these gases is generally half than the one in metal-organic frameworks or 3D covalent organic frameworks both on a gravimetric and a volumetric basis, with the exception of COF-8, which has an uptake comparable to other organic frameworks as far as methane adsorption is concerned.
We have investigated the mechanism of diffusion in order to assess similarities and/or differences with the behavior observed in carbon nanotubes, that have a similar pore structure and where transport is known to occur very rapidly. Our results point out that gas diffusion in 2D covalent organic frameworks is one order of magnitude more rapid than in metal-organic frameworks or zeolites, but still not as fast as in carbon nanotubes.
The adsorption and diffusion characteristics of these materials are related to the peculiar structure of the solid–fluid potential energy surface.

1. Introduction

Recent advances in the synthesis of metal-organic frameworks (MOF) with adjustable characteristics such as reticular symmetry and pore size [1–5] have led to a considerable interest in these materials for practical applications, mostly in the field of gas storage and separation due to the extremely low densities and high surface areas that characterize MOFs. Particular emphasis has been drawn to hydrogen and methane adsorption [6–10].

In parallel to the advancement of new techniques and protocols for the synthesis of MOFs, a large amount of work has been performed on the development of reliable computer models for studying the properties of these materials, with particular emphasis to gas adsorption. It has been shown that models based on transferable force fields are able to explain and predict adsorption isotherms of a wide variety of gases [11–14] and can be used to design new materials with the aim of optimizing methane or hydrogen storage [15–17]. Moreover computer simulations have been proved to be a good complement to the experimental efforts to improve the activation process of organic frameworks [18].

Much work has also been devoted to improve the accuracy of the force field: many groups have been using ab-initio techniques to calculate the interaction of hydrogen with the metal-organic framework known as MOF-5 (or IRMOF-1) [19–22]. These calculations have pointed out the importance of a correct treatment of the dispersion forces to correctly evaluate the magnitude of the hydrogen-framework interaction [21]. State of the art calculations based on the Møller–Plesset perturbation theory [19] show that the binding energy of hydrogen with MOF-5 is not too different from what can be predicted using transferable force fields. In fact one observes generally a good agreement between experimental adsorption isotherms and the results of computer simulations based on model potentials [13,18,23].

While the knowledge of the adsorption properties of metal-organic materials is steadily increasing, both from an experimental and computer simulation point of view, much less effort has been devoted to the study of diffusion and transport of gases, which play an important role in practical applications. The theory of gas diffusion within nanoporous materials has been developed and applied to the study of zeolites with particular emphasis to the possibility of obtaining efficient gas separation from a mixture, and many reviews are available on this subject, such as Refs. [24] and [25]. Early investigations on gas diffusion in MOFs have been focused in particular on hydrogen and methane [26–28], and it has been found that the magnitude of the self-diffusion coefficient is

* Corresponding author. Tel.: +39 0461 881583.
E-mail address: garberog@science.unitn.it (G. Garberoglio).

1387-1811/$ - see front matter © 2008 Elsevier Inc. All rights reserved.
doi:10.1016/j.micromeso.2008.05.023

comparable to what has been observed in silica zeolites, ranging from 1 to 10×10^{-8} m^2 s^{-1} at room temperature. Computer simulations of diffusion in MOFs, calculated using model potentials, compare favorably with the few available experimental results [29].

On the other hand the calculation of transport coefficients in carbon nanotubes has pointed out that in these materials diffusion coefficients might be up to three orders of magnitude higher than in other nanoporous materials. This outstanding performance of carbon nanotubes has been traced back to the presence of one-dimensional channels with almost no corrugation of the potential energy surface [30]. Moreover it has been shown that this rapid transport does not depend either on the assumed rigidity of the tubes [31] or on the nature of the adsorbate [32,33].

Very recently a new class of organic framework materials has been synthesized and characterized. Covalent organic frameworks (COF) are made up by organic linkers held together by boron-oxide clusters by means of covalent bonds [34,35]. COFs retain the good stability and pore-size adjustability of MOFs, and the absence of heavy metallic ions present in MOFs gives rise to very low densities. In fact one of the COFs, named COF-108, is the lightest crystalline material ever reported, with a density of 0.17 g cm^{-3}.

The reticular structure of COFs can be tailored in a wide variety of shapes, and materials composed by layers with hexagonal symmetry have recently been obtained [36]. The microscopic structure of these 2D COFs presents one-dimensional pores whose size can be varied in a wide range. Diameters between 8 and 32 Å, i.e. comparable with those of medium sized carbon nanotubes, have been reported.

As is well known the availability of a suitable atomic force fields which give a realistic description of the interaction of the materials with various sorbents, is an important achievement since most of the properties can be predicted by using computer simulation. In a previous work we have indeed performed computer simulations to show that 3D COFs [35] have the possibility of being very good sorbents for hydrogen and methane, outperforming the isoreticular MOFs and likely to meet or exceed the US Department of Energy target for methane adsorption at room temperature [37].

In view of the possible important applications of these novel materials for gas storage and separation, we believe it useful to carry out a detailed study of their properties concerning both adsorption and diffusion using the already tested classical force fields.

In the present work we have analyzed these properties for hydrogen and methane in the recently synthesized 2D COFs, in particular on the materials named COF-6, COF-8 and COF-10.

The first step is the comparison of the computer simulation (CS) of adsorption with experimental isotherms of Ar, in order to validate the force field. Then we evaluate the storage capacity of hydrogen and methane in these materials and compare it with the same quantity in other materials like MOF and carbon nanotubes.

Eventually we evaluate the self and transport diffusion coefficients and find that they are one order of magnitude higher than those calculated for MOFs. However a comparison with the diffusivity of these gases in carbon nanotubes shows that diffusion in 2D COFs is much slower.

A thorough comparison of the structure of the potential energy surface (PES) between COFs and nanotubes points out for the first time the origin of such a big difference.

2. Potential model and simulation details

The 2D COFs whose structure is shown in Fig. 1, have been treated as rigid crystals whose atomic coordinates were downloaded following the instruction reported in Ref. [36]. In order to calculate the solid–fluid potential energy we have used the DREIDING force field [38] together with the Lorentz–Berthelot combination rules and the Lennard-Jones potential parameters for the adsorbate that are reported in Table 1. The interaction has been truncated after a cutoff of 17 Å and long range corrections have not been applied.

In the case of hydrogen quantum diffraction effects have been taken into account by using the Feynman–Hibbs (FH) correction to the classical potential $v(\mathbf{x})$

$$v_{\mathrm{FH}}(\mathbf{x}) = v(\mathbf{x}) + \left(\frac{\hbar^2}{24\mu k_B T}\right)\nabla^2 v(\mathbf{x}) \tag{1}$$

In this equation μ is the reduced mass for two interacting particles: it has been set to half the hydrogen molecular mass when calculating the fluid–fluid interaction, and to the hydrogen molecular mass when calculating the solid–fluid interaction. It should be noted that taking only the quadratic term in the FH expansion in powers of $\hbar$ might not be sufficient if the size of the nanopores is comparable to the de Broglie wavelength of the molecule at the state point considered, and it has been shown that in this case quartic terms might be needed [43,44]. In our case the pore sizes are at least 8 Å wide to be compared with a de Broglie wavelength of H_2 at 77 K of Λ = 1.4 Å and hence we did not resort to the quartic approximation.

The solid–fluid interaction has been precalculated on a regular grid whose spacing has been set to 0.2 Å and 0.1 Å in the case of the classical and quantum potential, respectively. The solid–fluid potential at each point has been calculated during the simulation using three-dimensional cubic spline interpolation.

Adsorption isotherms were generated using the Grand Canonical Monte Carlo (GCMC) technique, using at least 4 million equilibration moves and 8 million production moves at each state point. Some simulations were performed with 10 million steps for equilibration and production to verify convergence.

The chemical potential used as input for the GCMC has been related to the pressure of the bulk fluid using the van der Waals equation of state whose parameters were chosen so that its critical point corresponds to the actual critical point of the gas under consideration [45].

The total amount of gas adsorbed per unit cell (N_{tot}) has been converted to excess adsorption using the formula [46]

$$N_{\mathrm{exc}} = N_{\mathrm{tot}} - \rho(T,P)V_{\mathrm{free}} \tag{2}$$

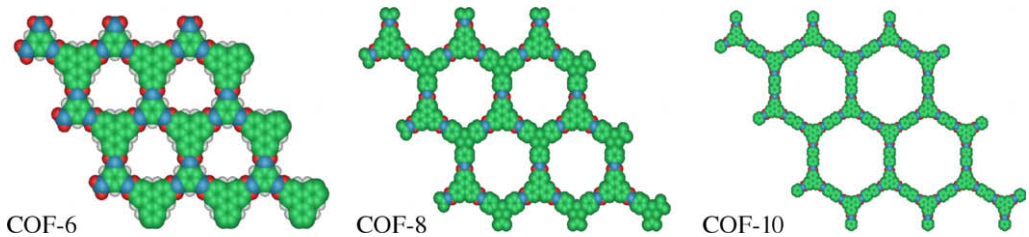

Fig. 1. The structure of the 2D COFs.

Table 1
Lennard-Jones parameters used in this work

Atom/molecule	ε/k_B (K)	σ (Å)
He [39]	10.22	2.556
Ar [40]	119.8	3.4
CH_4 [41]	148.0	3.73
H_2 [42]	34.2	2.96
B [38]	47.806	3.581
C [38]	47.856	3.473
H [38]	7.649	2.846
O [38]	48.158	3.033

Table 2
Unit cell masses, volumes and free volumes for the materials studied in this work

Material	Mass (g/mol unit cell)	Unit cell volume (Å^3)	Free volume (Å^3)	Density (g cm^{-3})
COF-6	425.8	660.0	275.9	1.07
COF-8	632.9	1523.4	884.7	0.69
COF-10	1121.6	3963.6	2973.8	0.47

where $\rho(T,P)$ represents the density at the given temperature obtained from the van der Waals equation and V_{free} is the free volume for adsorption. This latter quantity has been calculated as the volume within 1 unit cell where the potential energy of interaction of a Helium atom with the solid framework is less than 10^4 K. Values of the free volume and other relevant parameters for the materials studied in this work are reported in Table 2.

Well equilibrated configurations from GCMC at selected thermodynamic points have been used to perform molecular dynamics (MD) simulations. We have used a velocity Verlet integrator with a timestep of 1 fs and 3 fs for H_2 and CH_4, respectively. Runs of at least 200 ps were performed to equilibrate the system, and trajectories of at least 5 ns were used in the production phase. In some cases, especially at very low temperatures, runs as long as 30 ns were necessary to achieve a sufficiently good statistics. The simulation box was chosen at each thermodynamic point to be sufficiently large so to contain between 200 and 250 adsorbate particles. This was typically done by selecting the transverse size of the simulation box large enough to satisfy the cutoff requirement and extending it along the direction of the pores so that the desired number of molecules could be contained in equilibrium conditions.

The temperature has been fixed by using the technique of weak coupling to an external bath [47], with a time constant set to 1 ps during equilibration and to 100 ps during production. We have calculated the mean square displacement along the direction of the pore's axis (z) by averaging on at least 8 independent runs at each state point. The mean square displacement $\Delta z^2(t)$ is given by

$$\Delta z^2(t) = \left\langle \frac{1}{N} \sum_i |z_i(t+\tau) - z_i(\tau)|^2 \right\rangle \tag{3}$$

where $z_i(t)$ is the z coordinate of molecule i and the average is performed on the independent runs and the various starting times τ. N is the total number of molecules in the simulation box. The corresponding self-diffusion coefficient D_s for the motion along the one-dimensional pores has been calculated as

$$D_s = \lim_{t\to\infty} \frac{\Delta z^2(t)}{2t} \tag{4}$$

As is well known the self-diffusion coefficient D_s is related to transport (i.e. Fickian) diffusion in solids only in the limit of zero loading. At finite loadings the transport diffusion coefficient D_t is generally different from D_s but can still be calculated from equilibrium molecular dynamics simulations [24,25]. The transport diffusion coefficient is conveniently defined in terms of the corrected diffusivity D_0, as

$$D_t = D_0 \frac{\partial \ln f}{\partial \ln c}\bigg|_T \tag{5}$$

where f is the fugacity as a function of the concentration c of the adsorbed species. The partial derivative at constant temperature is known as the thermodynamic correction factor and can be derived from the knowledge of the adsorption isotherm. The corrected diffusivity is given by

$$D_0 = \lim_{t\to\infty} \frac{1}{2t} \left\langle \frac{1}{N} \left| \sum_i (z_i(t+\tau) - z_i(\tau)) \right|^2 \right\rangle \tag{6}$$

and can be thought of as the diffusion coefficient of the center of mass of all the molecules within the simulation box. The average in Eq. 6 has been calculated using at least 25 independent runs at each state point considered.

3. Adsorption

3.1. Argon

To the best of our knowledge the only experimental isotherms of adsorption in 2D COFs reported so far are those presented in Ref. [36], where 2D COFs have been characterized by analyzing Ar adsorption at $T = 87$ K. In order to check the degree of accuracy that can be expected from our model in this case, we report the results of our simulations under the same conditions in Fig. 2.

The overall agreement between computer simulations and experimental results is quite good. In particular the simulation can reproduce the Type IV isotherm behavior observed in COF-8 and COF-10, as well as the positions of the steps at $p \simeq 0.03$ bar for COF-8 and $p \simeq 0.25$ bar for COF-10. The Type I isotherm behavior observed for COF-6 is also reproduced. The larger discrepancy regards the saturation adsorption of COF-8 and COF-10 that is overestimated by 10% with respect to the experimental values. Nevertheless the agreement between simulation and experiment is better than what is observed in the case of 3D COFs, where simulations using the same force field as in this work overestimate the adsorption upon saturation by at least 25% [37].

The reason for the better performance of the same computer model in the case of 2D COFs with respect to the 3D counterparts

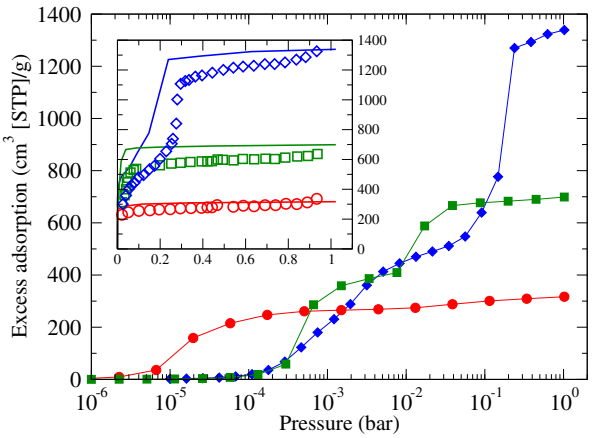

Fig. 2. Isotherm of adsorption of Ar in 2D COFs at $T = 87$ K from computer simulations. Circles: COF-6, squares: COF-8, diamonds: COF-10. Lines are a guide to the eye. Inset: the experimental isotherms of adsorption from Ref. [36] (open symbols) together with the simulation results (full lines).

can be due to the less compact structure of the former materials. In fact a detailed analysis of computer simulations of hydrogen adsorption in isoreticular MOFs [14] has shown that the amount of gas adsorbed is correlated, as the loading is increased, firstly to the isosteric heat of adsorption, then to the surface area of the sorbent and finally, near saturation conditions, to the free volume. All of these quantities are indeed related to properties of the PES. The isosteric heat at small loading (that is under the conditions where it is related to adsorption) depends on the binding energy [13], whereas the surface area and free volume depend on the geometry of the PES.

In view of these facts we suggest that the PES in the more compact 3D COFs emphasizes the discrepancies between the assumed and the actual form of the solid–fluid interaction. If this is the case one would expect the actual isotherms of adsorption in the low density 3D COFs (such as COF-105 and COF-108) to show a better agreement with the computer model than the ones of high density 3D COFs reported in Ref. [35].

Despite the differences between computer simulations and the real data, it is now well established that simulations based on classical force fields are an invaluable tool to characterize adsorption [12,13,18,37] and in some cases even design materials with a prescribed set of properties [15,17].

Finally we would like to point out that even if there is some discrepancy between the simulated and experimental results, a comparison between computer simulations is very likely to catch the general trend occurring in the behavior of actual materials. It is in this spirit that we now proceed to report and discuss the results of computer simulations of adsorption and transport in 2D COFs.

3.2. Hydrogen

The adsorption isotherms of hydrogen in 2D COFs at $T = 77$ K are reported in panel (a) of Fig. 3. The three isotherms show a maximum in the excess adsorption occurring around 25 bar for COF-6 and 45 bar for COF-8 and COF-10. The material with the largest adsorption per unit mass is COF-10, where hydrogen adsorption reaches 4.2 wt%, followed by COF-8 and COF-6. The amount of hydrogen adsorbed upon saturation is lower than the amount adsorbed in 3D COFs, which can be as high as 10.5% [37], and in MOFs, where values as high as 7.5% are observed in computer simulations [19,13].

There are two main reasons for the inferior adsorption performance of 2D COFs when compared to other covalent or metal-organic frameworks: (i) as it can be seen from Table 2, the densities of the 2D COF materials are comparable, if not larger, than the densities of other organic frameworks [13,37] and hence, from a gravimetric point of view, 2D COFs, and COF-6 in particular, experience some disadvantages. (ii) The structure of 2D COFs is such that adsorption can occur only along the surface of the one-dimensional pores, resulting in a smaller surface area with respect to 3D organic frameworks. In fact the experimental surface areas for 2D COFs studied in this article range from 965 to 1050 $m^2\,cm^{-3}$ [36], to be compared with the values in the range 1425–1600 $m^2\,cm^{-3}$ for 3D COFs [35] and the values of 1710 and 2050 $m^2\,cm^{-3}$ for IRMOF-1 [6] and IRMOF-6 [8], respectively.

As a consequence the adsorption of hydrogen in 2D COFs is correspondingly lower than the one observed in 3D COFs and MOFs, either on a gravimetric or volumetric basis. In fact the maximum excess volumetric adsorption at $T = 77$ K from computer simulation turns out to be in the range 230–310 $cm^3(STP)\,cm^{-3}$ for 2D COFs, to be compared with the values of 410 $cm^3(STP)\,cm^{-3}$ and 470 $cm^3(STP)\,cm^{-3}$ calculated for IRMOF-1 and COF-102, respectively, [48].

The same behavior is observed when the adsorption of hydrogen at $T = 298$ K is analyzed, as it is shown in panel (b) of Fig. 3.

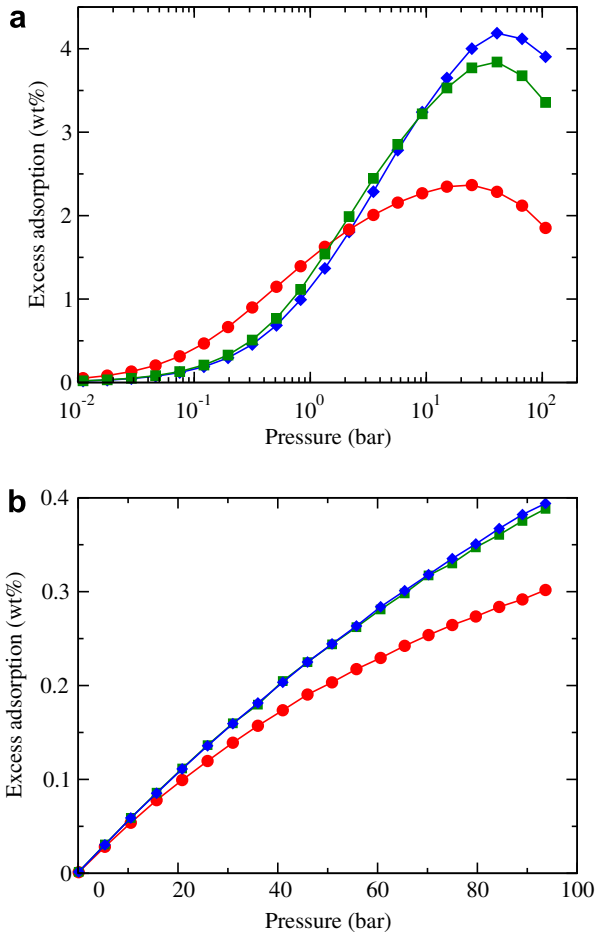

Fig. 3. Isotherm of adsorption of H_2 in 2D COFs at $T = 77$ K (a) and $T = 298$ K (b). Circles: COF-6, squares: COF-8, diamonds: COF-10. Lines are a guide to the eye.

The amount of hydrogen adsorbed on a gravimetric basis at the pressure of $p = 100$ bar is half of that adsorbed in 3D COFs, where adsorption reaches 0.8 wt% [37], and it is less than one order of magnitude than the US Department of Energy target of 6 wt%.

3.3. Methane

The adsorption of methane in 2D COFs at room temperature, reported in Fig. 4, follows the same general trends observed in the case of hydrogen. The performance of these materials is generally worse than the one of other organic frameworks, even if COF-8 is comparable to IRMOF-1 and IRMOF-6 [15]. None of the 2D COFs reaches the US Department of Energy target of 167 $cm^3(STP)\,cm^{-3}$ at $p = 35$ bar [49], which is met by the 3D COFs, even if the uptake of methane on COF-8 can be as high as 155 $cm^3(STP)\,cm^{-3}$ at $p \simeq 75$ bar.

The analysis of the adsorption isotherms of methane shows with great clarity the different adsorption properties of the three COFs studied in this work, and the relation between adsorption and the structure of the PES [13,14,37,50]. We notice that COF-6 is the most adsorbing material at pressures lower than $p = 20$ bar. This is due to the fact that the more compact structure of COF-6, with respect to COF-8 and COF-10, enhances the binding energy of the adsorption sites, because more atoms contribute with their attractive potential tails to lowering the energy in the positions where the PES has a minimum (i.e. near the B atoms, see the discussion in Section 4.1). A higher binding energy results then in a larger adsorption at low pressures [13,14,37]. As the pressure is increased, however, methane rapidly saturates the smaller

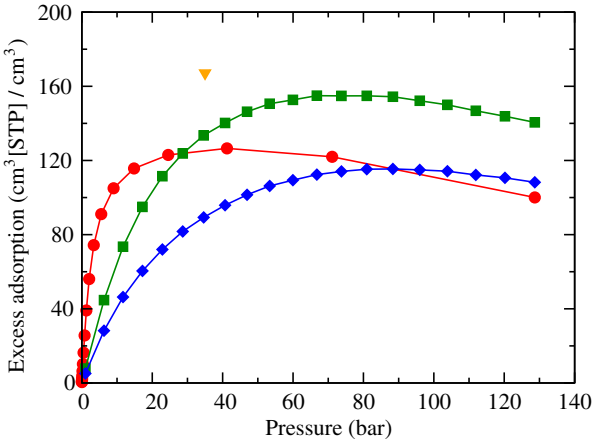

Fig. 4. Isotherm of adsorption of CH_4 in 2D COFs at $T = 298$ K. Circles: COF-6, squares: COF-8, diamonds: COF-10. The triangle denotes the US Department of Energy target reported in Ref. [49]. Lines are a guide to the eye.

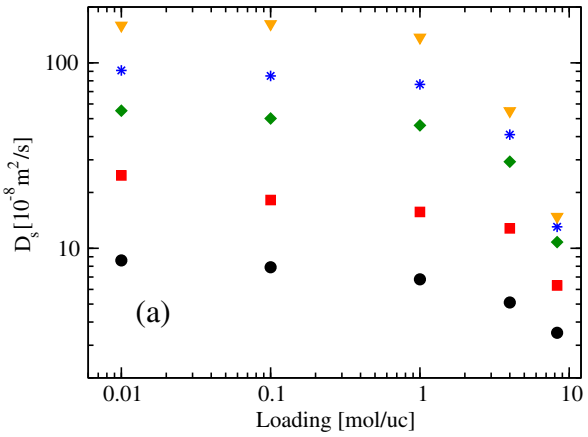

Fig. 5. Values of the self-diffusion coefficient D_s for H_2 in COF-10 as a function of loading and temperature. The circles, squares, diamonds, stars and triangles correspond to the temperatures of 77, 100, 150, 200 and 298 K, respectively. The loading of 1 mol/unit cell corresponds to a pressure $p = 10$ bar at $T = 298$ K, and to a pressure $p = 1$ bar at $T = 77$ K.

pores of COF-6. The opposite behavior is observed in COF-10, the material with the largest pore structure: the binding energy is smaller than in COF-6 and hence one observes a smaller Henry constant in the linear regime at low pressure. As the pressure is increased, however, the adsorbate can fill the larger pores and hence the quantity of methane adsorbed becomes higher (on a volumetric basis) then what can be adsorbed in COF-6.

The material called COF-8 shows an intermediate behavior at low pressure, on account of its pore size, which is between the dimensions of the pores in COF-6 and COF-10. As the pressure is raised, however, COF-8 shows a larger affinity to methane than the other two materials. This is due to the fact that the pores are not so small to saturate quickly as in COF-6, but neither so big to leave large voids within the unit cell with small attraction between the adsorbent and the adsorbate, as it happens in COF-10. The net result is that COF-8 shows the largest amount of methane adsorbed upon saturation, but does not reach the performance of the 3D covalent frameworks at $p = 35$ bar.

A similar behavior is observed also in the case of hydrogen adsorption (cfr. Fig. 3), even though the smaller size and the weaker interaction with the framework of this latter molecule tends to minimize the differences between the various materials, and especially those between COF-8 and COF-10.

4. Self-diffusion and transport

We report in Fig. 5 the self-diffusion coefficient D_s defined in Eq. 4 as a function of loading at different temperatures in the case of hydrogen adsorbed in COF-10.

As is evident the diffusion coefficient increases as the loading is decreased, approaching a plateau value whose value raises with the temperature. In fact in the limit of zero pressure the single particle dynamics is ruled by the solid–fluid interaction only and, as the loading is increased, the single particle motion becomes progressively hindered by the presence of a growing number of neighbors and, correspondingly, the self-diffusion coefficient becomes smaller.

At each temperature the values of the self-diffusion coefficient are two orders of magnitude smaller than the corresponding values in carbon nanotubes where, in the limit of zero loading, values of D_s as high as 10^{-3} m^2 s^{-1} have been calculated at room temperature [30]. In the limit of high loading the self-diffusion coefficient in carbon nanotubes has been found to drop by more than two orders of magnitude, reaching the value of $\simeq 2 \times 10^{-6}$ m^2 s^{-1}, still an order of magnitude higher than the value $\simeq 10^{-7}$ m^2 s^{-1} that we have observed in 2D COFs at the same temperature (see Fig. 5).

Table 3
Values of the self-diffusion coefficient D_s of hydrogen and methane in 2D COFs

Adsorbate	Adsorbent	Loading (mol/unit cell)	Temperature (K)	D_s (10^{-8} m^2 s^{-1})
H_2	COF-6	0.01	77	4
H_2	COF-6	4	77	1
H_2	COF-6	0.01	298	43
H_2	COF-6	4	298	7.5
H_2	COF-10	0.01	77	8.5
H_2	COF-10	8	77	3.5
H_2	COF-10	0.01	298	160
H_2	COF-10	8	298	15
CH_4	COF-6	0.01	100	0.45
CH_4	COF-6	1	100	0.27
CH_4	COF-6	0.01	298	7.9
CH_4	COF-6	1	298	3.3
CH_4	COF-10	0.01	77	0.1
CH_4	COF-10	8	77	0.03
CH_4	COF-10	0.01	298	22.5
CH_4	COF-10	8	298	7.7

Nevertheless the self-diffusion coefficient of hydrogen is still higher than the one observed in 3D organic frameworks. In the limit of zero loading the self-diffusion coefficient for hydrogen in IR-MOF-1 (MOF-5) has been calculated to reach the value of $\simeq 2 \times 10^{-7}$ m^2 s^{-1} at room temperature [27], which is an order of magnitude smaller than in the case of 2D COFs. The self-diffusion coefficient of hydrogen in isoreticular MOFs has been predicted to be in the range $1-3 \times 10^{-8}$ m^2 s^{-1} at $T = 77$ K [28], and very recent computer simulations provide a value in the same range for a new organic framework, Zn(bdc)(ted)$_{0.5}$ [23].

These values are comparable with our findings in the case of hydrogen diffusion in COF-6, reported in Table 3, but are lower than the values observed in COF-10, where the diffusion coefficient is in the range $3.5-8.5 \times 10^{-8}$ m^2 s^{-1} at $T = 77$ K and in the range $1.5-16 \times 10^{-7}$ m^2 s^{-1} at $T = 298$ K.

The self-diffusion coefficient of methane in 2D COFs is also larger than that in other organic frameworks. Skoulidas and Sholl [27] reported values in the range $2-3 \times 10^{-8}$ m^2 s^{-1} for diffusion in IR-MOF-1 at room temperature. Our results, reported in Table 3, show that methane diffusion in IRMOF-1 is comparable with diffusion in COF-6 and it is definitely slower than the diffusion observed in COF-10, where our calculated values for D_s are in the range $7.7-22.5 \times 10^{-8}$ m^2 s^{-1}, depending on the loading.

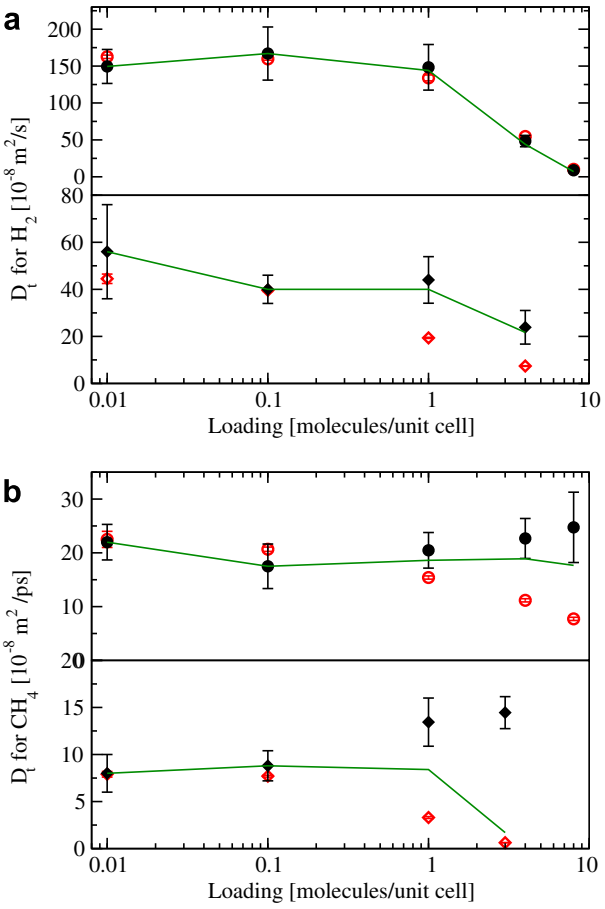

Fig. 6. The transport diffusion coefficient D_t for hydrogen (a) and methane (b) in COF-10 (filled circles) and COF-6 (filled diamonds) at $T = 298$ K. The open symbols refer to the self-diffusion coefficient D_s at the same thermodynamic points. The line joins the values of D_0.

In Fig. 6a and b we compare the self-diffusion coefficient D_s with the transport diffusion coefficient D_t evaluated according to Eq. 5 for H_2 and CH_4 at room temperature, respectively. Similarly to what has been observed in the case of self-diffusion, transport diffusion in 2D COFs is generally more rapid than in other organic frameworks [27,23], particularly in the case of COF-10, where D_t is an order of magnitude higher than in MOFs.

In the case of H_2 both the self and transport diffusion coefficient decrease as the loading is increased, whereas in the case of CH_4 the self-diffusion is observed to decrease at higher loadings while the transport diffusion increases.

In the case of H_2 one does not reach the saturation region even at the highest pressures investigated here (the more so for COF-10, see Fig. 3) and therefore the thermodynamic correction factor is at most 1.2. Moreover D_0 is found to follow the same trend as D_s, i.e. a progressive decrease at increasing loading. The same behavior has been observed for transport diffusion in MOFs [27,23], where the difference between self and transport diffusion of hydrogen is apparent only at very high loadings when the saturation regime is approached.

The situation of CH_4 is found to be different in two ways. For methane in COF-6 one reaches saturation already at a loading of 3 molecules per unit cell, and under these conditions the thermodynamic correction factor plays a relevant role being of the order of 8.5. In all the other cases the corrected diffusivity D_0 is found to remain almost constant in the whole loading range and the increase of D_t is entirely due to the presence of the thermodynamic correction factor.

The same qualitative behavior of the diffusion coefficients as a function of increasing loading, i.e. a decrease of the self-diffusivity D_s, a less marked decrease of the corrected diffusivity D_0 and a general increase of the transport diffusion coefficient D_t has been already observed and discussed in the case of diffusion of light gases in silicalite [51] as well as in MOFs [27].

4.1. Mechanism of diffusion in 2D COFs

We wish to clarify now the reason for the large difference between the values of the self-diffusion coefficient of hydrogen in nanotubes and 2D COFs. Despite the similar topology of the two systems, which present large one-dimensional pores, we demonstrate that the structure of the solid–fluid PES is responsible for the different diffusion properties.

As is well known PES corrugation in carbon nanotubes is negligible, and in fact the presence of very small potential barriers for the motion along the tube axis has been indicated as the principal reason for the rapid transport of hydrogen and methane in this system [30,31]. In fact we have calculated the size of the corrugation effects in the case of hydrogen interacting with a (10,10) carbon nanotube and found that near the position of the radial minimum of the PES, where the density of adsorbed species is concentrated, the motion along the tube axis does not meet potential barriers higher than 10–20 K, which are easily crossed at room temperature.

In the case of diffusion along the pores in 2D COFs the situation is very different and the motion along the pores is highly hindered by the structure of the PES: there are quite large potential barriers to be overcome and diffusion along the pores' direction (the z axis) takes place by jumps separated by quite long residence times. This can be seen in Fig. 7, where we report the z coordinate of a hydrogen molecule as a function of time, together with the value of the corresponding solid–fluid potential energy.

As is apparent the molecule passes rather long times with almost a constant value of the z coordinate, as it is evidenced by the vertical dashed bars in the figure. During the same periods the potential energy of interaction remains generally quite low, indicating that the particle moves near one of the binding sites. On the other hand it is easily seen that the displacement along the axis is correlated with high values of the potential energy, a signature of the presence of quite large barriers that must be overcome for the molecule to diffuse.

Indeed the analysis of the PES isosurfaces sheds more light on the actual mechanism of diffusion, confirming the scenario illustrated so far. We report in Fig. 8 three isosurfaces for the interac-

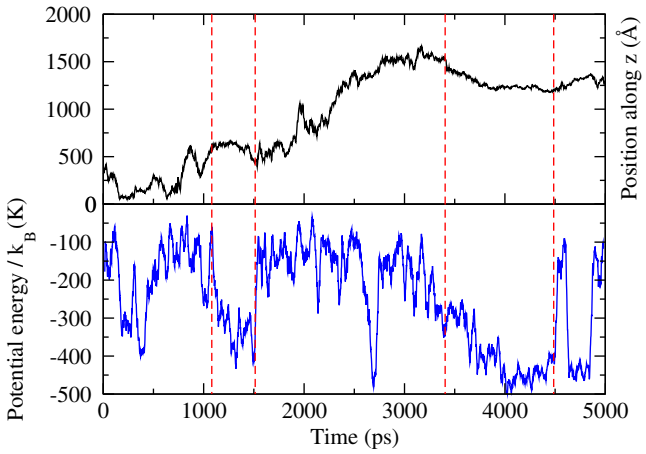

Fig. 7. Position along the z axis (top) and solid–fluid potential energy (bottom) in the dynamics of a single H_2 particle adsorbed within COF-10 at $T = 200$ K.

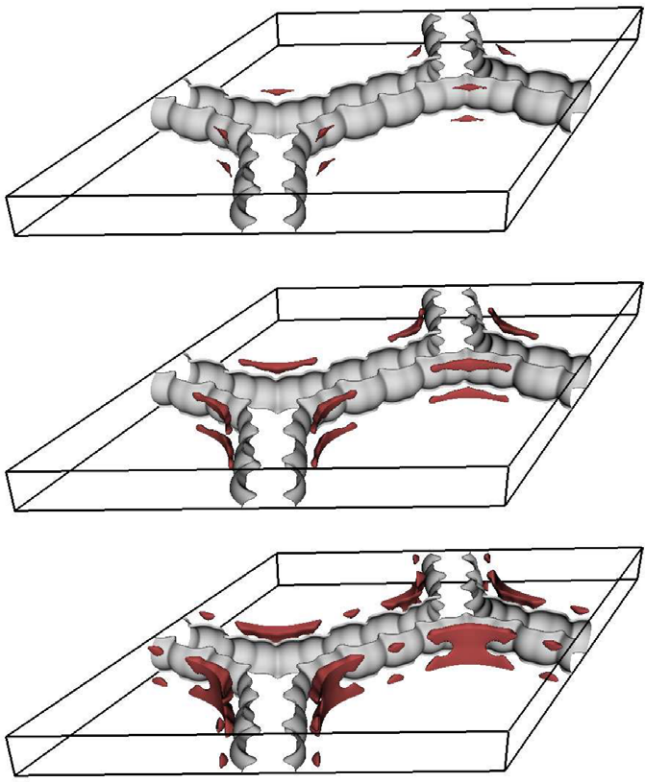

Fig. 8. Isosurfaces of the solid–fluid potential energy of interaction U_{SF} of H_2 with COF-10. The light gray surface corresponds to $U_{SF}/k_B = 10^5$ K and the dark gray surface corresponds to (from top to bottom) the values $U_{SF}/k_B = -620$ K, $U_{SF}/k_B = -540$ K and $U_{SF}/k_B = -450$ K, respectively. The thick lines show the boundary of the unit cell of the crystal.

tion of hydrogen with COF-10. The minima of the PES at $U_{SF} = -620$ K are very close to the vertices of the hexagons which form the cross-section of the pores. The isosurfaces form isolated pockets until the solid–fluid potential reaches the value of $U_{SF} = -450$ K, when the isosurface extends through all the pore along the z direction. One can then calculate the activation energy for diffusion along z to be of the order of $\Delta E = 170$ K, much larger than the size of the PES corrugation in carbon nanotubes, and comparable with the value of the kinetic energy for the motion along z at room temperature.

Visual inspection of the PES isosurfaces shows that the most probable paths for diffusion along z pass through few specific regions on the isosurface at $U_{SF} = -450$ K, located in the vicinity of the corners of the hexagons. Therefore this cross-sectional effect further reduces the probability of a particle to move along the pore axis, and contributes to lowering the value of the diffusion coefficient.

Indeed it is to the very presence of corners in the pore cross-section that one can trace back the appearance of pronounced minima in the PES. In fact the solid–fluid potential near the corners is determined by the overlap of the attractive parts of the atoms placed on the two intersecting edges, whereas only the atoms on one edge contribute to the PES along the organic linker. Notice that in the force field that we have used the values of the Lennard-Jones interaction energy of boron, carbon and oxygen are nearly the same and in the range $\varepsilon/k_B = 47.8$–48.2 K (see Table 1). Hence the appearance of local minima near the corners is a purely geometric effect and does not depend on the different chemical composition of the metal-oxide corner with respect to the organic linker. Indeed a similar structure of the PES is obtained using the Universal Force Field [52], which assigns less similar values of the interaction parameter ε to boron, carbon and oxygen.

In the case of carbon nanotubes the disposition of carbon atoms around the pore does not present corners and hence the solid–fluid PES is less corrugated, resulting in negligible barriers for diffusion.

5. Conclusions

We have presented computer simulation results of adsorption and diffusion of hydrogen and methane in recently synthesized 2D COFs using the DREIDING force field. Our results point out that the amount of hydrogen adsorbed in these materials is generally half the amount adsorbed in other organic frameworks under the same conditions, either on a gravimetric or a volumetric basis. The adsorption of methane is also generally less than in other materials with the exception of COF-8. We have traced back the origin of this behavior to the structure of the solid–fluid PES of 2D COFs.

We have also calculated self and transport diffusion coefficients of hydrogen and methane, and we found that diffusion in these materials can occur up to one order of magnitude faster than in other organic frameworks but not quite as rapidly as in carbon nanotubes, despite the similar topological structure of these two systems.

By analyzing the PES isosurfaces we have shown that the reason of the performance of 2D COFs can be ascribed to the fact that diffusion along the pores of the 2D COFs is activated. The existence of deep wells in the PES is traced back to the presence of corners in the cross-section of the one-dimensional pores. The height of the energy barrier in 2D COFs is smaller than in other frameworks, and hence diffusion is faster, but it is still comparable to the average kinetic energy at room temperature, whereas the corrugation of the PES of carbon nanotubes along the tube direction does not exceed few tens of Kelvin.

Acknowledgments

We thank Prof. A. Miotello for useful discussions. The computer simulations have been performed on the HPC facility *Wiglaf* of the Department of Physics, University of Trento.

References

[1] H. Li, M. Eddaoudi, M. O'Keeffe, O.M. Yaghi, Nature 402 (1999) 276.
[2] M. Eddaoudi, H.L. Li, O.M. Yaghi, J. Am. Chem. Soc. 122 (2000) 1391.
[3] O.M. Yaghi, M. O'Keeffe, N.W. Ockwig, H.K. Chae, M. Eddaoudi, J. Kim, Nature 423 (2003) 705.
[4] F. Fajula, A. Galarneau, F. Di Rienzo, Micropor. Mesopor. Mater. 82 (2005) 227.
[5] S.L. James, Chem. Soc. Rev. 32 (2003) 276.
[6] M. Eddaoudi, J. Kim, N. Rosi, D. Vodak, J. Wachter, M. O'Keefe, O.M. Yaghi, Science 295 (2002) 469.
[7] N.L. Rosi, J. Eckert, M. Eddaoudi, D.T. Vodak, J. Kim, M. O'Keeffe, O.M. Yaghi, Science 300 (2003) 1127.
[8] J.L. Rowsell, A.R. Millward, K.S. Park, O.M. Yaghi, J. Am. Chem. Soc. 126 (2004) 5666.
[9] M. Hirscher, B. Panella, Scripta Mater. 56 (2007) 809.
[10] X. Lin, J. Jia, P. Hubberstey, M. Schröder, N.R. Champness, Cryst. Eng. Commun. 9 (2007) 438.
[11] A. Vishnyakov, P.I. Ravikovitch, A.V. Neimark, M. Bulow, Q.M. Wang, Nano Lett. 3 (2003) 713.
[12] L. Sarkisov, T. Düren, R.Q. Snurr, Mol. Phys. 102 (2004) 211.
[13] G. Garberoglio, A.I. Skoulidas, J.K. Johnson, J. Phys. Chem. B 109 (2005) 13094.
[14] H. Frost, T. Düren, R.Q. Snurr, J. Phys. Chem. B 110 (2006) 9565.
[15] T. Düren, L. Sarkisov, O.M. Yaghi, R.Q. Snurr, Langmuir 20 (2004) 2683.
[16] T. Sagara, J. Ortony, E. Ganz, J. Chem. Phys. 123 (2005) 214707.
[17] H. Frost, R.Q. Snurr, J. Phys. Chem. C 111 (2007) 18794.
[18] J. Liu, J. Culp, S. Natesakhawat, B.C. Bockrath, B. Zande, S.G. Sankar, G. Garberoglio, J.K. Johnson, J. Phys. Chem. C 111 (2007) 9305.
[19] T. Sagara, J. Klassen, E. Ganz, J. Chem. Phys. 121 (2004) 12543.
[20] T. Mueller, G. Ceder, J. Phys. Chem. B 109 (2005) 17974.
[21] A. Samanta, T. Furuta, J. Li, J. Chem. Phys. 125 (2006) 084714.
[22] T. Yildrim, M.R. Hartman, Phys. Rev. Lett. 95 (2005) 215504.
[23] J. Liu, J.Y. Lee, L. Pan, R.T. Obermyer, S. Simizu, B. Zande, S.G. Sankar, J.K. Johnson, J. Phys. Chem. C 112 (2008) 2911.
[24] D. Dubbeldam, R.Q. Snurr, Mol. Simul. 33 (2007) 305.
[25] D.S. Sholl, Acc. Chem. Res. 39 (2006) 403.
[26] A.I. Skoulidas, J. Am. Chem. Soc. 126 (2004) 1356.

[27] A.I. Skoulidas, D.S. Sholl, J. Phys. Chem. B 109 (2005) 15760.
[28] Q. Yang, C. Zhong, J. Phys. Chem. B 109 (2005) 11862.
[29] F. Stallmach, S. Gröger, V. Künzel, J. Kärger, O.M. Yaghi, M. Hesse, U. Müller, Angew. Chem., Int. Edit. 45 (2006) 2123.
[30] A.I. Skoulidas, D.M. Ackerman, J.K. Johnson, D.S. Sholl, Phys. Rev. Lett. 89 (2002) 185901.
[31] H. Chen, J.K. Johnson, D.S. Sholl, J. Phys. Chem. B 110 (2006) 1971.
[32] H. Chen, D.S. Sholl, J. Am. Chem. Soc. 126 (2004) 7778.
[33] A.I. Skoulidas, D.S. Sholl, J.K. Johnson, J. Chem. Phys. 124 (2006) 054708.
[34] A.P. Côté, A.I. Benin, N.W. Ockwig, M. O'Keeffe, A.J. Matzger, O.M. Yaghi, Science 310 (2005) 1166.
[35] H.M. El-Kaderi, J.R. Hunt, J.L. Mendoza-Cortés, A.P. Côté, R.E. Taylor, M. O'Keeffe, O.M. Yaghi, Science 316 (2007) 268.
[36] A.P. Côté, H.M. El-Kaderi, H. Furukawa, J.R. Hunt, O.M. Yaghi, J. Am. Chem. Soc. 128 (2007) 12914.
[37] G. Garberoglio, Langmuir 23 (2007) 12154.
[38] S.L. Mayo, B.D. Olafson, W.A. Goddard III, J. Phys. Chem. 94 (1990) 8897.
[39] J. de Boer, A. Michels, Physica 5 (1938) 945.
[40] G.C. Maitland, M. Rigby, E.B. Smith, W.A. Wakeham, Intermolecular Forces: Their Origin and Determination, Clarendon Press, Oxford, 1981.
[41] S.J. Goodbody, K. Watanabe, D. MacGowan, J.P.R.B. Walton, N. Quirke, J. Chem. Soc., Faraday Trans. 87 (1991) 1952.
[42] V. Buch, J. Chem. Phys. 100 (1994) 7610.
[43] A.V. Anil Kumar, S.K. Bhatia, Phys. Rev. Lett. 95 (2005) 245901.
[44] A.V. Anil Kumar, H. Jobic, S.K. Bhatia, J. Phys. Chem. B 110 (2006) 16666.
[45] J.O. Hirschfelder, C.F. Curtiss, R.B. Byrd, Molecular Theory of Gases and Liquids, John Wiley & Sons, 1954.
[46] A.L. Myers, AIChE J. 48 (2002) 145.
[47] H.J.C. Berendsen, J.P.M. Postma, W.F. van Gunsteren, A. DiNola, J.R. Haak, J. Chem. Phys. 81 (1984) 3684.
[48] STP: Standard Temperature and Pressure, 10^5 Pa and 273.16 K.
[49] T. Burchell, M. Rogers, SAE Tech. Pap. Ser., 2000, 2000–01–2205. Please notice that the definition of STP reported in this paper is 1 atm and 298 K. We have corrected the target value of 180 cm^3 [STP]/cm^3 to match the current IUPAC definition used here [48].
[50] T. Düren, F. Millange, G. Férey, K.S. Walton, R.Q. Snurr, J. Chem. Phys. C 111 (2007) 15350.
[51] A.I. Skoulidas, D.S. Sholl, J. Phys. Chem. B 106 (2002) 5058.
[52] A.K. Rappé, C.J. Casewit, K.S. Colwell, W.A. Goddard III, W.M. Skiff, J. Am. Chem. Soc. 114 (1992) 10024.